Intermediate State in Type-I Superconductors

1 author:

V. Kozhevnikov
56 PUBLICATIONS **337** CITATIONS

SEE PROFILE

We are IntechOpen, the first native scientific publisher of Open Access books

3,350
Open access books available

108,000
International authors and editors

1.7 M
Downloads

151
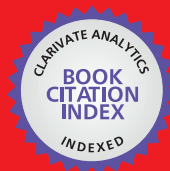Countries delivered to

Our authors are among the

TOP 1%
most cited scientists

12.2%
Contributors from top 500 universities

CLARIVATE ANALYTICS
BOOK CITATION INDEX
INDEXED

WEB OF SCIENCE™

Selection of our books indexed in the Book Citation Index
in Web of Science™ Core Collection (BKCI)

Interested in publishing with us?
Contact book.department@intechopen.com

Intermediate State in Type-I Superconductors

Vladimir Kozhevnikov

Additional information is available at the end of the chapter

Abstract

Intermediate state in type-I superconductors is one of the oldest challenges of superconductivity put forward by Gorter and Casimir, Pearls, F. London, and Landau back in the 1930s. In this chapter, we review the main properties of this state and principal theoretical approaches to interpret them. Recent experimental and theoretical achievements in this field are discussed in more details.

Keywords: type-I superconductors, intermediate state, thermodynamic properties, magnetization

1. Introduction

Intermediate state (IS) is defined as a thermodynamically equilibrium state in which a type-I superconductor is split for domains of superconducting (S) and normal (N) phases [1–3]. For completeness of description, we begin with a brief overview of properties of the Meissner state, which will be necessary for discussion of the IS properties.

1.1. Meissner state in cylindrical specimens

Consider a specimen of a type-I superconductor at temperature $T < T_c$ in a free space (vacuum) subjected to a uniform magnetic field $H < H_{cr}(T)$, where T_c is critical temperature at zero field and $H_{cr}(T)$ is critical field of the S/N transition at given T. (We use notation H_{cr} instead of commonly used H_c because the latter is reserved for thermodynamic critical field, which can be different from H_{cr}). Assume that the specimen is a long cylinder with a circular base of radius $R \gg \lambda$ (λ is the penetration depth) and H is parallel to the cylinder as shown in **Figure 1a**. A demagnetizing factor η [2, 4] of such a specimen is zero, which means that outside it $B = H_i = H$ (we use CGS units) all the way down to the sample surface.
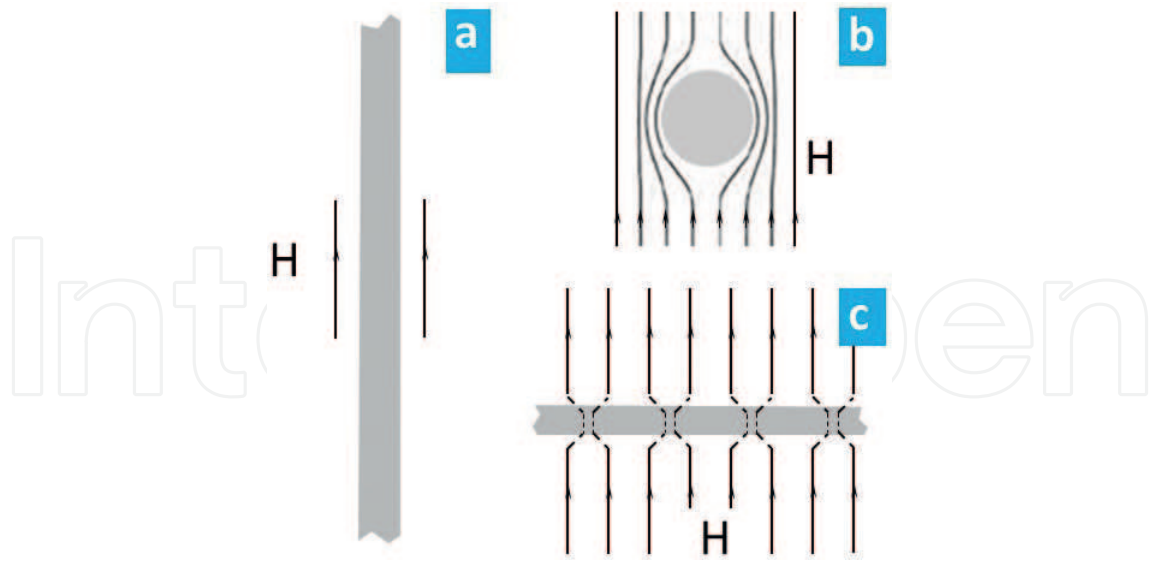
Figure 1. Cross-sectional view of specimens (shown in gray) with demagnetizing factor $\eta = 0$ (a), $\eta = 1/2$ (b), and $\eta = 1$ (c) in a weak magnetic field H. In (a) and (b) the specimen (a cylinder) is in the Meissner state; in (c) the specimen (an infinite slab) is in the intermediate state starting from any H exceeding zero.

Here B is magnetic induction or magnetic flux density [5] or merely B-field [6]. B is an average microscopic magnetic field available for measurements [2]. H_i is magnetic field strength, also referred as magnetic and magnetizing force [4], Maxwell field [7], thermodynamic field [8], magnetic field [5], H-field [6], and others. And H is applied field set by a magnet power supply (for simplicity we will ignore a small contribution of Earth magnetism); it is the field away from the specimen or the field which would be in a space occupied by the specimen if the latter is absent. Away from the specimen, H_i is identical to H, but it can be not so near and inside the specimen. Everywhere outside the specimen, $B = H_i$ because magnetic permeability of the free space, as well as permeability of the N phase in superconductors, $\mu \equiv B/H_i$ is unity by definition.

Our cylindrical specimen is in the Meissner state, implying that inside it $B = 0$ and $H_i = H$ due to continuity of the tangential component of this field [9]. A jump of induction at the specimen surface $\Delta B = H$ means that there is a surface current I, in which linear density $g \equiv I/l = \Delta Bc/4\pi = cH/4\pi$, where l is length of the specimen and c is speed of light. This surface current is regarded as a screening current protecting the specimen interior from the external field. Taking into account direction of $\mathbf{g}$ ($= \mathbf{n} \times \mathbf{H}c/4\pi$, where $\mathbf{n}$ is the unit vector normal to the surface and directed outward), we arrive at a well-familiar formula for the specimen magnetic moment M:

$$M = -gl\frac{A}{c} = \left(\frac{cH}{4\pi}l\right)\frac{A}{c} = -\frac{H}{4\pi}V, \tag{1}$$

where A and V are the base area and volume of the specimen, respectively.

The same result follows from definition of the field strength:

$$H_i \equiv B - 4\pi m, \tag{2}$$

where m is magnetization, which in superconductors is a *macroscopic* average of the magnetic moment per unit volume $m = M/V$ and, as it was mentioned above, $H_i = H$ due to geometry of our specimen.

Thermodynamics of our and any other singly connected superconductor can be described using total free energy $\tilde{F}_M(T, V, H)$, which differential $d\tilde{F}_M(T, V, H)$ is [2].

$$d\tilde{F}_M = -SVdT - \mathbf{M} \cdot d\mathbf{H}, \tag{3}$$

where S is entropy per unit volume and a small variation of V due to changing magnetic field is neglected.

Integrating Eq. (3) at constant temperature, we arrive at another well-known and very important formula for the total free energy of the singly connected superconductors in magnetic field [1, 2]:

$$\left(\tilde{F}_M\right)_{sH} = \left(\tilde{F}_M\right)_{s0} - \int_0^H \mathbf{M} \cdot d\mathbf{H} = \left(\tilde{F}_M\right)_n - \frac{H_c^2}{8\pi}V - \int_0^H \mathbf{M} \cdot d\mathbf{H}, \tag{4}$$

where $\left(\tilde{F}_M\right)_{s0}$ is the total free energy of the S state in zero field, $\left(\tilde{F}_M\right)_n$ is the total free energy of the N state, and $\left(H_c^2/8\pi\right)V$ is the condensation energy, where H_c is thermodynamic critical field. Note that, since M in the N state is zero (because μ of the N phase is unity), the total free energy for this state does not depend on the field. This means that $\left(\tilde{F}_M\right)_n = F_{n0}$ and $\left(\tilde{F}_M\right)_{s0} = F_{s0}$, where F_{n0} and F_{s0} are Helmholtz free energies $F(T, V, B)$ in the normal and superconducting states at zero field, respectively.

Importance of Eq. (4) is associated, firstly, with the fact that neither $\left(\tilde{F}_M\right)_n$ nor the condensation energy $\left(H_c^2/8\pi\right)V$ depends on the specimen shape, and therefore Eq. (4) is valid for singly connected specimens of *any* shape. Secondly, Eq. (4) explicitly shows that the extra total free energy (above the free energy of the ground state $\left(\tilde{F}_M\right)_{s0}$) is the specimen magnetic energy $E_M = - \int_0^H \mathbf{M} \cdot d\mathbf{H}$, representing energy of interaction of the external field H with the specimen magnetic moment M induced by this field. More specifically, E_M is kinetic energy of electrons (Cooper pares) carrying the induced currents [1]. And thirdly, Eq. (4) shows that the source of E_M is condensation energy. Finiteness of the later makes transition to the N state a mandatory property of any superconductor [2]. At the S/N transition, the magnetic energy of any specimen equals to its condensation energy, or area under $M(H)$ curve plotted as $4\pi M/V H_c$ vs. H/H_c, when $\mathbf{M}$ is aligned to $\mathbf{H}$, is 1/2.

This as-called rule of 1/2 (or in general case Eq. (4)), represents the energy balance or the first law of thermodynamics for singly connected superconductors at constant temperature; compliance with this rule/equation is a necessary condition for discussion of equilibrium properties of superconductors [1].

Using Eq. (1) for M of our cylindrical sample, we rewrite Eq. (4) as

$$\tilde{F}_M(H) = F_n - \frac{H_c^2}{8\pi}V + \frac{H^2}{8\pi}V. \tag{5}$$

Now a question arises; up to what fields Eq. (1) is valid? Vast majority of superconductors are of type II, for which Eq. (1) holds up to a low critical field $H_{c1} < H_{cr}$ and $H_{cr} = H_{c2}$, which is an upper critical field. However there is a relatively small group of mostly pure elementary materials, for which Eq. (1) (or the Meissner condition $B = 0$) holds in the entire field range of the superconducting state, i.e., up to H_{cr}. Those are type-I superconductors. An example of $M(H)$ dependences for a typical type-I superconductor with $\eta = 0$ is shown in **Figure 2**.

S/N transition takes place when free energies of the S and N states are equal, i.e., $\tilde{F}_M(H_{cr}) = (\tilde{F}_M)_n$. For our type-I cylindrical sample, as seen from Eq. (5), this implies that $H_{cr} = H_c$ and therefore the S/N transition in specimens with $\eta = 0$ must be discontinuous, i.e., thermodynamic phase transition of the first order, in full agreement with experimental results, e.g., with those shown in **Figure 2**.

1.2. Intermediate state

Now, we turn our cylinder perpendicular to the applied field. In a weak field, the specimen is in the Meissner state (inside it $B = 0$), but the pattern of field lines looks now as shown in **Figure 1b**. The external field near the specimen is tangential to its surface, which follows from always valid conditions of continuity of the normal component of B and of tangential component
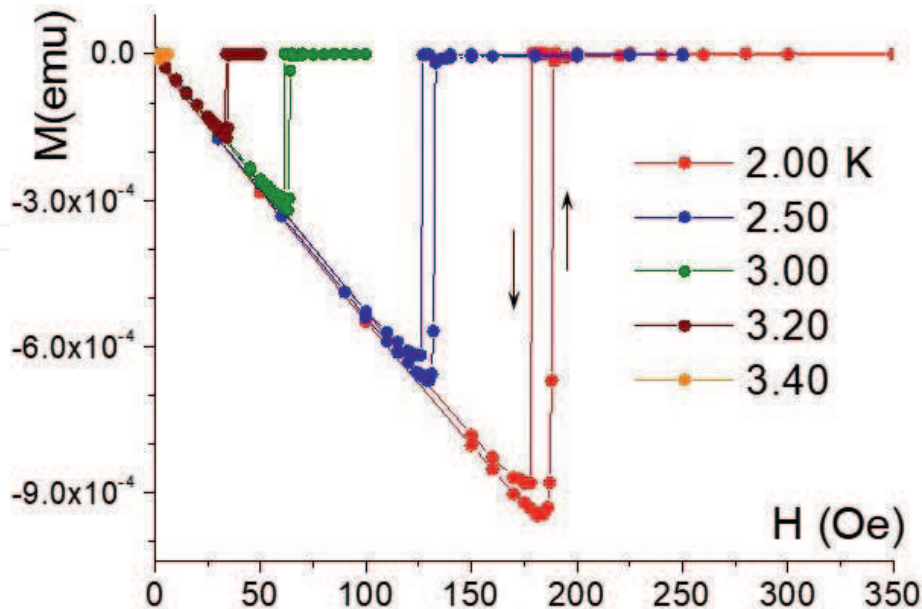

Figure 2. Experimental data for magnetic moment of a pure indium film 2.79 μ m thick measured in parallel applied field H at indicated temperatures. Errors up and down indicate that the measurements were conducted at increasing and decreasing field, respectively.

of H_i [2, 4]. Indeed, our cylindrical specimen in perpendicular field in the Meissner state represents a uniformly magnetized ($B = const = 0$) prolate ellipsoid with $\eta = 1/2$ [2, 4]. Inside of any uniform ellipsoid, H_i is also uniform, and when **H** is parallel to an axis of ellipsoid with respect to which the demagnetizing factor is η, the fields H_i, B, and H are connected with each other as.[1]

$$(1 - \eta)H_i + \eta B = H. \tag{6}$$

Hence, the field H_i inside our specimen in the Meissner state is $H/(1 - \eta)$, and therefore H_i on the external side of the specimen surface (the external field) is

$$H_i = H sin\theta/(1 - \eta), \tag{7}$$

where θ is the angle between the normal and the applied field **H**.

Therefore near the "poles" of our specimen the field is zero, whereas near "equator" it is twice as big as the applied field. This implies that the external field near "equator" reaches the critical value H_c at $H = H_c(1 - \eta) = H_c/2$. When H is increased beyond this value, the field must enter the specimen destroying superconductivity. However, contrarily to the previous (parallel) case, superconductivity cannot be destroyed completely because there is still plenty of condensation energy left in the specimen.

Indeed, the specimen magnetic moment $M \equiv (B - H_i)V/4\pi = -HV/4\pi(1 - \eta) = -HV/2\pi$; therefore magnetic energy E_M at $H = H_c/2$ is

$$E_M = -\int_0^{0.5H_c} \mathbf{M} \cdot d\mathbf{H} = \frac{VH_c^2}{16\pi} < \frac{VH_c^2}{8\pi}. \tag{8}$$

Hence, as seen from Eq. (4), $\tilde{F}_M < (\tilde{F}_M)_{n'}$ and therefore the specimen must remain superconducting.

At the first sight, one might expect that at $H > H_c(1 - \eta)$, the field will gradually enter the specimen, thus destroying superconductivity over the field range from $H_c(1 - \eta)$ to H_c. The superconducting cylinder in such case would stay resistanceless with gradually changing volume of the S core as shown in **Figure 3**. However, this scenario is problematic because as soon as the field enters the specimen, the density of the field lines near the "equator" decreases and hence the field inside the convex blue region in **Figure 3** becomes smaller than H_c. Then this region should go back to the S state.[2] This means that when $H > H_c(1 - \eta)$, the ellipsoidal specimen splits into S and N regions, as it was suggested for the first time by Gorter and Casimir [10].

---

[1]Derivation of Eq. (6) can be found in [2]; Maxwell using it in [4] refers to Poisson.
[2]Historically impossibility of configuration like that shown in **Figure 3** was explained basing on a paradigm of instability of the N phase against transforming to the S phase at $H_i < H_c$ (see, e.g. [8]). However, this (the N phase at $H_i < H$) *does take place* in specimens in the IS, but only at H_i in the upper part of the IS field range. At the lower edge of this range (at $H = (1 - \eta)H_c$) B in the first N domain and therefore H_i throughout the specimen is always H_c.
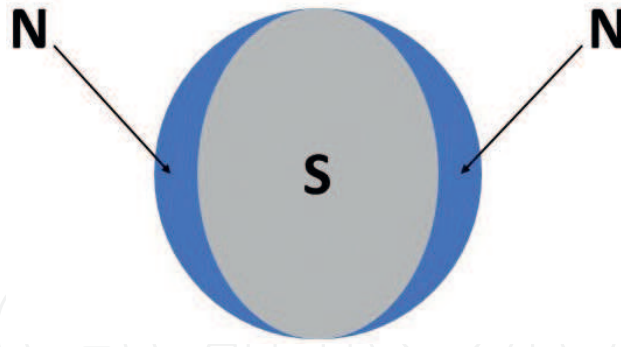
Figure 3. Cross section of the cylindrical sample in case if superconducting phase (S, colored in gray) is gradually replaced by the normal (N, colored in blue) phase filled by the field.

After Peierls [11] this inhomogeneous state in type-I superconductors is named the intermediate state. Properties of the IS were (and in some extent still are) one of the longest-standing challenges of physics of superconductivity. Below we will expose the main theoretical ideas and key experimental achievements addressing these properties. Comprehensive reviews of the experimental and theoretical works on the IS published before 1970 are available in [1, 12, 13]; for references to more recent publications, we recommend papers by Brandt and Das [14] and Clem et al. [15].

2. Model of Peierls and London

The first successful theoretical model of the IS magnetic properties was developed in 1936 independently by Peierls [11] and London [16]. In this model properties of ellipsoidal samples are considered in an averaged limit, in which the nonuniform induction B is replaced by average $\overline{B}$. This allowed to use Eq. (6) with demagnetizing factor η calculated for uniform ellipsoid. However Eq. (6) has two unknowns, B and H_i, both of which are needed to calculate the specimen magnetic moment. Basing on a paradigm that the N phase is unstable at $H_i < H_c$, Peierls and London *postulated* that inside the specimen in the IS (i.e., at $(1 - \eta)H_c < H < H_c$),

$$H_i = H_c. \tag{9}$$

Eqs. (2), (6), and (9) constitute a complete system of equations. Solving it one finds B, H_i, and M:

$$H \leq H_c(1 - \eta) \begin{cases} B = 0 \\ H_i = H/(1 - \eta) \\ M = HV/4\pi(1 - \eta) \end{cases} \tag{10}$$

$$H_c(1 - \eta) \leq H \leq H_c \begin{cases} \overline{B} = (H - H_c(1 - \eta))/\eta \\ H_i = H_c \\ M = V(H - H_c)/4\pi\eta \end{cases}. \tag{11}$$

Graphs of these functions for $\overline{B}$ and M are shown in **Figure 4** in reduced coordinates. It is important that area under the graphs for $4\pi M(H)/VH_c$ vs. H/H_c is the same 1/2. Therefore this model meets the necessary thermodynamic condition of Eq. (4). The PL model fits well experimental data obtained for thick specimens, i.e., when the field inhomogeneities near the surfaces through which the flux enters and leaves the specimen are negligible. Overall, the PL model represents a global description of the IS in zero-order approximation [8]. Similar model for the mixed state in type-II superconductors is available in [17]. For type-I superconductors this new model converts to the model of Peierls and London.

3. Landau laminar models

Magnetic flux structure of the IS was for the first time considered by Landau [18] for an infinite parallel-plane plate (slab) in perpendicular field, i.e., for the sample-field configuration shown in **Figure 1c**. In such a specimen the surface current (and hence the Meissner state) is absent because $\overline{B} = H$, and therefore $g = (H - \overline{B})c/4\pi = 0$ at any H from zero to H_{cr}. Due to that the IS starts at H right above zero, no matter how small is this field. Magnetic moment of this specimen (Landau considered thick plate) is $M(H) = (-H_c + H)V/4\pi$; graphs for $\overline{B}$ and M are shown by the green lines in **Figure 4a** and **b**.

Assuming that (i) the plate is split for regularly structured S and N laminae and (ii) the boundary of a cross section of the S laminae is the line of induction B with magnitude H_c at the S/N interface, Landau calculated shape of rounded corners of the S laminae near the sample surface. Landau's scenario for cross section of the S-lamina near the surface is shown in **Figure 5a**. To meet the second assumption, Landau splits a central field line for two branches (*oba* and *ocd* in **Figure 5a**) making a sharp (90°) turn at the splitting point (*o*). Hence, in this scenario the field fills *all* space outside the specimen, as it is supposed to be the case in magnetostatics. On the other hand, splitting the field line challenges the magnetostatics rules [4], and the sharp turn of the line may cost the system too much energy [2, 19].
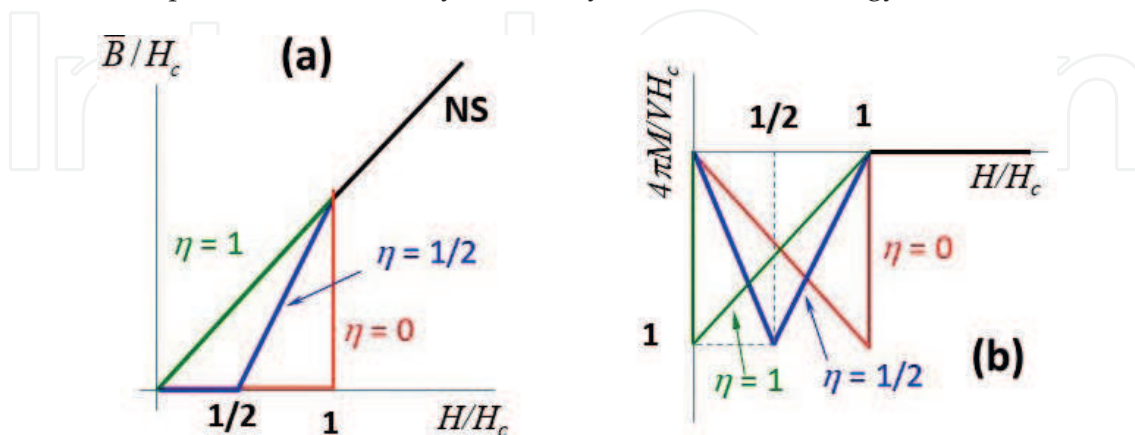

Figure 4. Peierls and London model. Average magnetic induction (a) and magnetic moment (b) for specimens with demagnetizing factor $\eta = 1$ (infinite slab in perpendicular field, green line), $\eta = 1/2$ (long cylinder in perpendicular field, blue line) and $\eta = 0$ (long cylinder in parallel field, red line). NS designates the normal state (black line).
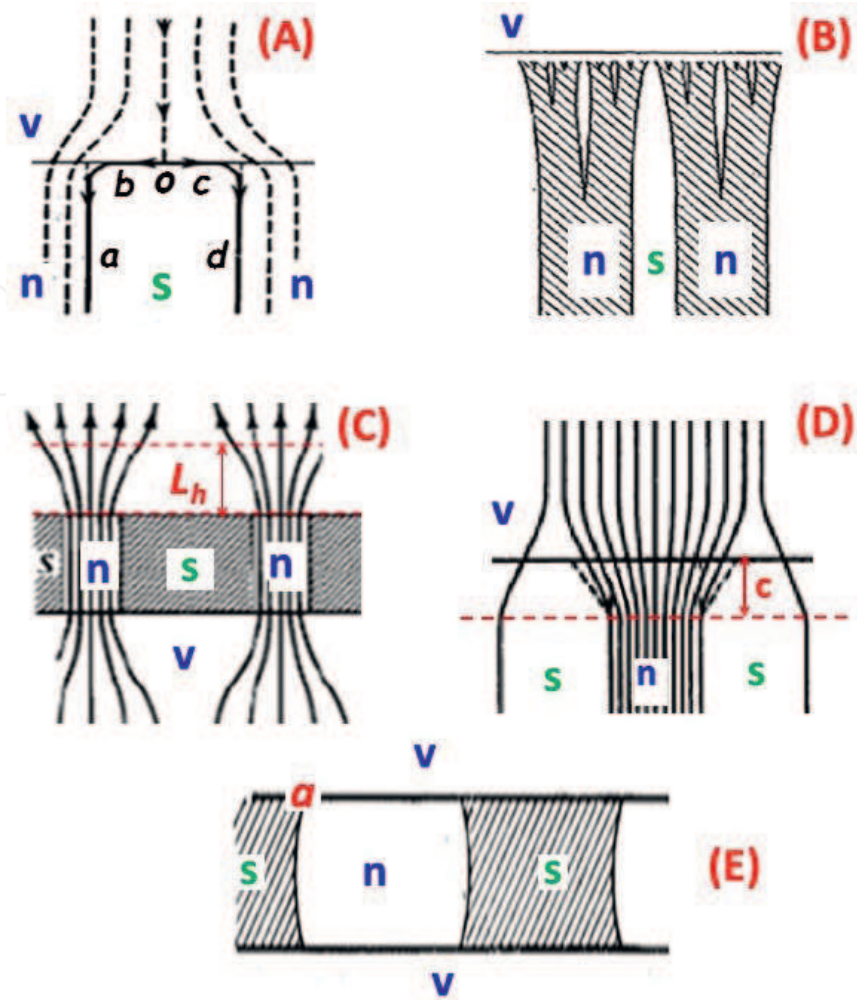
Figure 5. Cross-sectional views of the S and N laminae and of the field distribution (in A, C, and D) near the surface(s) of a type-I plane-parallel slab in perpendicular magnetic field. (A) Landau [18], (B) Landau [19], (C) Tinkham [3], (D) Abrikosov [7], and (E) Marchenko [20]. Letters s and n designate superconducting and normal phases, respectively; v designates the free space. In (C) v also designates a void in the static field outside the sample. See text for other notations.

The rounded corners and the field inhomogeneity near the surface yield an excess energy of the system favoring to a fine laminar structure (directly proportional to a period D of the one-dimensional laminar lattice). On the other hand, there is an excess energy associated with the surface tension at the S/N interface in the bulk, which favors to a coarse structure (reversely proportional to D). Optimizing sum of these two energy contributions in the specimen free energy, Landau calculated the period:

$$D^2 = \frac{\delta d}{f_L(h)},$$ (12)

where δ is a wall-energy parameter characterizing the S/N surface tension and associated with the coherence length [2, 3] and $f_L(h)$ is the Landau spacing function determined by the shape of the corners and the near-surface field inhomogeneity and $h = H/H_c$. $f_L(h)$ was calculated numerically in [21], and an analytical form of this function was obtained in [22] (see also [2]).

Soon thereafter Landau abandoned this model, admitting that the proposed flux structure does not correspond to a minimum of the free energy [23]. So, he suggested another so-called

branching model [19, 23] (see also [1, 8]), in which N laminae near the surface split for many thin branches as shown in **Figure 5B**, so that the flux emerges from the sample uniformly over the whole surface. However, this branching model was disproved by Meshkovskii and Shalnikov when they for the first time directly measured flux structure of the IS [24].

4. Other versions of near-surface properties

One of the important consequences of the Landau models is demonstration of significance of the near-surface field distribution and domain shape (FDDS) for forming and stabilizing the flux structure of the IS. On that reason it is worth to briefly overview other available scenarios for FDDS.

There are two simplified modifications of the original (non-branching) Landau's version of FDDS.

Tinkham [3] proposed that the dominant contribution in the surface-related properties comes from field inhomogeneities outside the sample extending over a "healing length" L_h as shown in **Figure 5C**. $L_h = \left(D_n^{-1} + D_s^{-1}\right)^{-1}$, where D_n and D_s are the widths of the normal and superconducting laminae, respectively. Correspondingly, Tinkham neglects the roundness of the laminae corners (*b* and *c* in **Figure 5A**). This version meets the limiting cases—$D \to 0$ when either $D_s \to 0$ or $D_n \to 0$—and is consistent with images of the IS flux structure (see, e.g., [13, 24, 25]). Tinkham's FDDS works surprisingly well for the IS [25, 26]; it was also successfully validated for the mixed state in type-II superconductors [27]. Note that all of these are in spite of apparent contradiction of the Tinkham's scenario with basics of magnetostatics, since it allows for existence of voids in the static magnetic field near the sample (e.g., in a region designated by *v* in **Figure 5C**).

Abrikosov [7] proposed another simplified version of Landau's FDDS. He assumed that major role is played by the round corners and therefore neglected the field inhomogeneity outside the specimen. However, the latter means that the field near the surface is uniform, and therefore this scenario is inconsistent with images of the IS flux structure. Abrikosov's version of FDDS is shown in **Figure 5D**, where size of the corners *c* is the same as L_h in the Tinkham's scenario.

An interesting result for a possible domain shapes was obtained by Marchenko [20]. Like Landau [18], Marchenko used conformal mapping to calculate the domain shape in infinite slab but in a tilted field. He found that in a *strongly tilted* field width of the S-domains can increase as shown in **Figure 5E**. We note that in such case, the field lines should leave the N domains converging instead of diverging as in **Figure 5A–D**, because bending of the lines over sharp corners (marked *a* in **Figure 5E**) would take enormous energy [2]. Therefore this scenario also allows for existence of the voids in the field outside the specimen; and moreover, it may lead to appearance of a maximum in the field magnitude in the free space above the N laminae.

To conclude this section on theoretically predicted scenarios for the near-surface properties of the IS, we note that neither of them is consistent simultaneously with the classical magneto-statics and with experimental images of the flux structure. So far no experimental results on

FDDS in the IS have been reported. Hence measurements of these properties are open and important (see, e.g., Landau's papers [18, 19, 23]) problem of fundamental superconductivity[3].

5. Key experiments

Although we began this chapter from theoretical models, a real story of the IS has started from experiment. Measuring electrical resistance R of tin wires, De Haas with collaborators revealed a strong dependence of $R(H)$ on direction of the applied field H: instead of a sharp S/N transition at a threshold field (H_c) in the parallel field, R returns to its full value gradually at the field range from about $H_c/2$ to H_c when the field is perpendicular [29, 30]. Later it was shown that reproducible $R(H)$ in the perpendicular field is liner [28]; one of the graphs for $R(H)$ from [28] is reproduced in **Figure 6**. The linear $R(H)$ is consistent with the Peierls-London model; however, it was revealed that transition from the Meissner state to the IS takes place at H_I, which is somewhat greater than $(1 - \eta)H_c =0.5H_c$.

The first observation of the IS magnetic structure was achieved by Meshkovsky and Shalnikov, who mapped the field in a gap between two tin hemispheres with radius 2 cm using a resistive probe made of a tiny bismuth wire [24]. Originally this experiment was designed to verify the
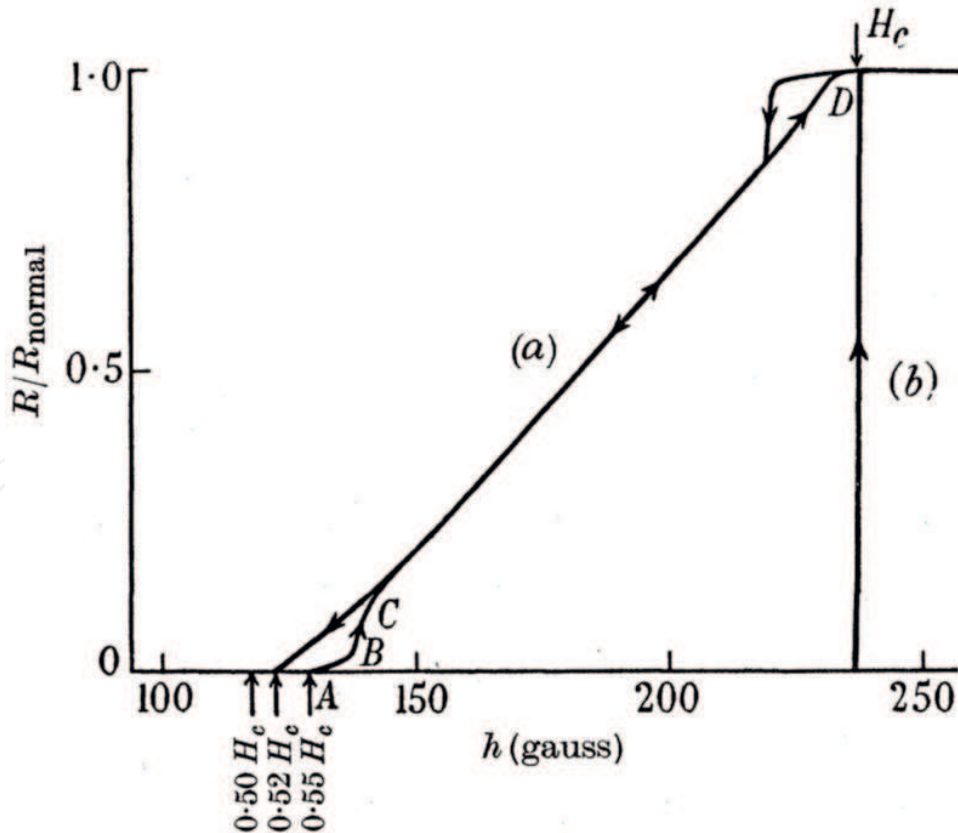

Figure 6. Relative resistance of a high-purity tin cylindrical wire of 0.4 mm in diameter and 5 cm in length at temperature 1.666 K (a) in increasing and in decreasing transverse field and (b) in increasing longitudinal field. After Andrew [28].

---

[3]First results of direct measurements of FDDS were recently presented in V. Kozhevnikov, A. Suter, T. Prokscha, C. Van Haesendonck arXiv:1802.08299v1 [cond-mat.supr-con] (2018).

Landau branching model, according to which the field near the surface is uniform and the flux structure can be observed only in a narrow gap inside the specimen provided the gap width is less than some critical value estimated by Landau [19]. It turned out that there is no critical gap and the field is inhomogeneous both inside (in the gap) and outside the specimen. These results unambiguously turned down the branching model. Typical images and diagrams for the field distribution obtained by Meshkovsky and Shalnikov are available in [1].

Further progress in imaging the IS structure was reached using Bitter or powder technique and magneto-optics [13]. It was established that the flux pattern in flat plates in perpendicular field consists of irregular corrugated laminae transforming into N (S) fractional laminae and tubes near the low (high) end of the IS field range. A numerous variety of different flux patterns were reported when samples are in nonequilibrium state [12].

A detailed study of the IS flux pattern was conducted by Faber with tin and high-purity aluminum parallel-plane plate specimens [31]. It was found that at high reduced temperature ($\approx 0.9 T_c$) in a broad field range, the structure is pass-independent (i.e., reproducible at increasing at decreasing fields) and consists of corrugated laminae. Therefore Faber concluded that the laminar flux structure is equilibrium structure of the IS. Typical images of the pass-independent flux pattern in perpendicular field from the Faber's work are shown in **Figure 7**.

A breakthrough in forming *regular and controllable* IS flux structure was achieved by Sharvin [32]. Applying the field tilted with respect to a single-crystal Sn specimen, Sharvin obtained a regular linear laminar structure as shown in **Figure 8**. Measuring period of the structure and using Landau's formula, Eq. (12), corrected to account the field inclination, Sharvin calculated the wall-energy parameter δ. Similar experiments and calculations Sharvin performed for In [32].

The aforementioned difference between the critical field H_I observed in resistive measurements and theoretically expected value for this field $(1 - \eta)H_c$ was investigated by Desirant and Shoenberg in a detailed study of magnetization of long cylindrical specimens of different radii in transverse field [33]. Apart from confirmation of the resistive results, Desirant and
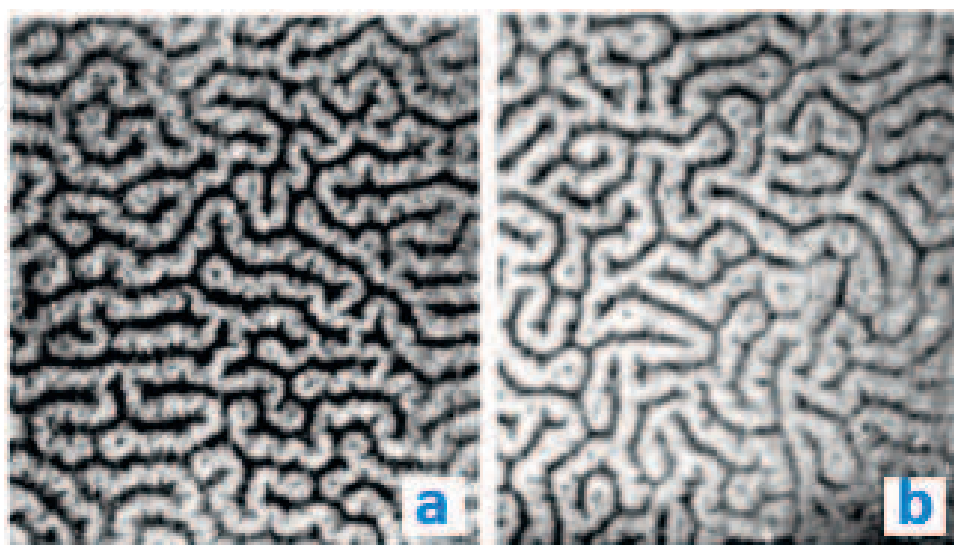

Figure 7. Typical images of pass-independent flux structures of the IS obtained with aluminum parallel-plane plate specimen in perpendicular field at temperature $0.92 T_c$ and the field $0.38 H_c$ (a) and $0.53 H_c$ (b). Dark areas are superconducting. After Faber [31].

Shoenberg revealed that the critical field of the IS/NS transition H_{cr} is appreciably smaller than the thermodynamic critical field H_c measured in parallel field. It was also found that the differences $\Delta H_I = H_I - (1 - \eta)H_c$ and $\Delta H_{cr} = H_c - H_{cr}$ depend on the specimen radius: the smaller the radius, the greater the differences. One of magnetization curves reported in [34] is reproduced in **Figure 9**.
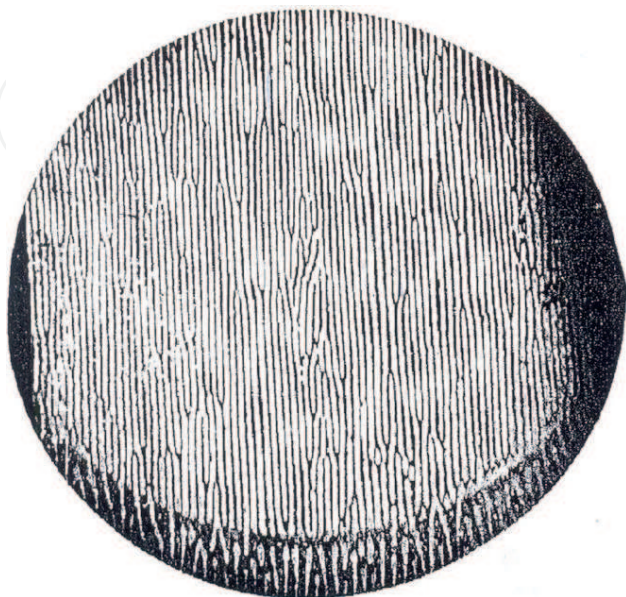

Figure 8. Photograph of the IS flux structures taken with a single-crystal tin disc-shaped specimen (Ø 50 × 2 mm²) in the field tilted for 15° with respect to the specimen at temperature $0.58T_c$ and field $0.95H_c$. Light areas are normal. After Sharvin [32].
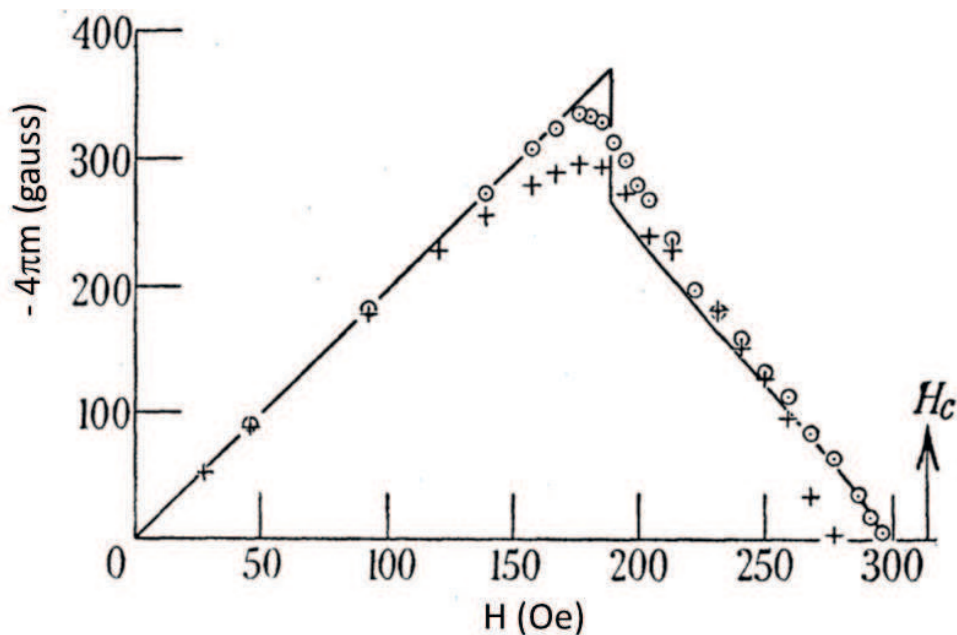

Figure 9. Magnetization curve ($m = M/V$) of cylindrical mercury specimen with radius 23 μm in transverse field at temperature 2.12 K measured at increasing (⊙) and decreasing (+) fields. H_c is thermodynamic critical field measured in parallel field. Solid line based on landau branching model [19] with wall-energy parameter adjusted for best fit. After Desirant and Shoenberg [34].

The differences of ΔH_I and ΔH_{cr} are usually interpreted as a price paid by the specimen for the extra energy needed to create the S/N interfaces in assumption that ΔH_I and ΔH_{cr} are small [3, 8]. We note that this explanation is not full because significant part of the extra free energy is associated with the field inhomogeneity near the specimen surface. On the other hand, the observed extension of the Meissner state (up to $H_I > (1 - \eta)H_c$) means that $4\pi M/V$ at H_I is greater than H_c, the value following from the PL model. This "excess magnetic moment" is consistent with the rule of 1/2, and it is indeed seen in **Figure 9** and in other data reported by Desirant and Shoenberg. However this feature can hardly be attributed to the S/N surface tension.

Egorov et al. [35] measured induction B in the bulk of N domains of a high-purity single-crystal tin slab ($18 \times 12 \times 0.56$ mm^3) in perpendicular field using μSR spectroscopy. Reported results are shown in **Figure 10**. H_t in this graph corresponds to H_{cr} in our notations. The tubular phase mentioned in the caption most probably corresponds to the filament state discussed in [36].

Results of Egorov et al. show that B in N domains is H_c at low applied field and decreases with increasing field down to H_{cr} at the IS/N transition. But induction B in N domains equals to the field strength H_i. Therefore the original postulate used in the PL and Landau models ($H_i = H_c$) is correct for the low reduced fields, but it can be not so at higher fields.

Recently the IS problem was revisited by Kozhevnikov et al. [25, 26] via magneto-optics and measurements of electrical resistivity and magnetization in high-purity indium films of different thickness in the fields of different orientations. An immediate motivation for this research was discrepancy in values of the coherence length for Sn and In following from Sharvin's results for the IS structure [32, 33] and those obtained from the measured magnetic field profile in the
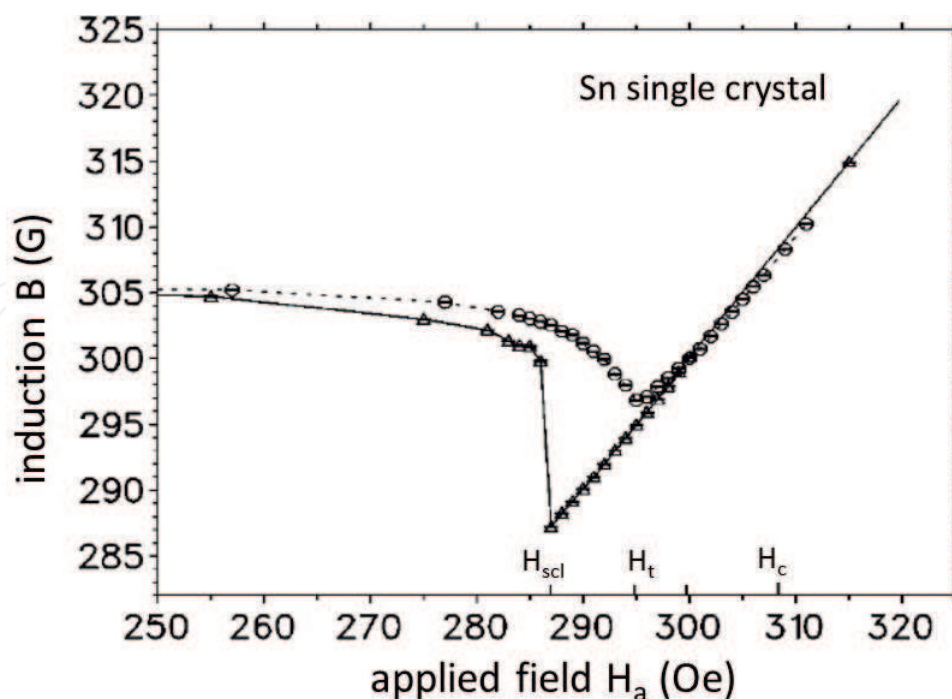
Figure 10. Induction in N domains of the Sn single-crystal plate at temperature 0.08 K measured at increasing (circles, solid line) and decreasing (triangles, dashed line) applied field. For decreasing field the N state is field supercooled down to H_{scl}. At increasing field the laminar structure transforms to one with tubular S regions at H_t. After Egorov et al. [35].

Meissner state [37]. In **Figure 11** we reproduce typical magneto-optical images obtained for a 2.5-μm-thick film. The most unexpected result revealed with this specimen is that in perpendicular field the critical field $H_{cr} \approx 0.4H_c$ at $T \to 0$. A typical magnetization curve obtained with another (3.86-μm-thick) film is shown in **Figure 12**. H_{cr} for this specimen at 2.5 K is $0.65H_c$ and
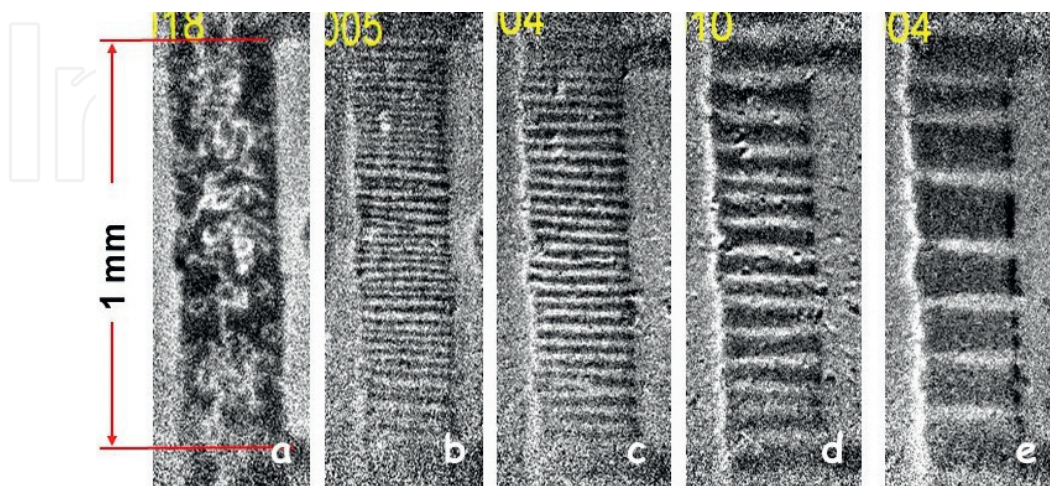

Figure 11. Magneto-optical images taken with 2.5-μm-thick in film at 2.5 K. [$H_\parallel$, $H_\perp$ in Oe]: (a) [0, 1], (b) [60, 8], (c) [100, 6], (d) [110, 3], and (e) [115, 1.3]. Superconducting regions are black. After Kozhevnikov et al. [25].
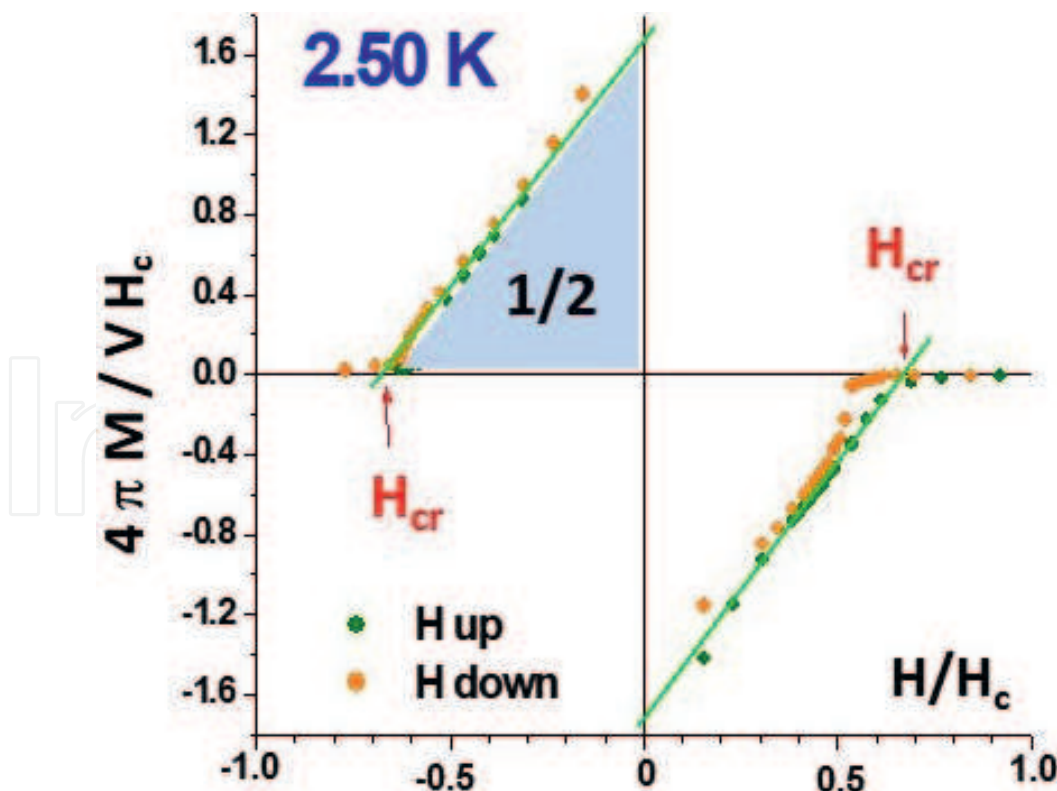
Figure 12. Magnetization curve of 3.86-μm-thick indium film measured in perpendicular field at 2.5 K. Green (orange) circles represent the data measured at increasing (decreasing) field. Shadowed area represents the specimen condensation energy (1/2 in the reduced coordinates of this graph). H_c was determined from magnetization curve in parallel field, and the specimen volume was determined from the slope of that curve. After Kozhevnikov et al. [25].

$4\pi M(0)/V = 1.6H_c$. All data were well reproducible, and the area under magnetization curves plotted in reduced coordinate is close to 1/2, meaning that the obtained experimental results reflect the equilibrium properties of the IS. However these results conflict with available theoretical models. A new model, consistently addressing outcomes of this work and explaining earlier revealed "anomalies," is presented in [25, 26]. We discuss it in the following section.

6. Laminar model for flat slab in tilted field

The simplest of experientially observed equilibrium domain structures of the IS is one-dimensional laminar lattice in slab-like specimens placed in a tilted field. Therefore such a specimen/field configuration is the most convenient for modeling. A laminar model for tilted field (LMTF) was developed in [25, 26]. Schematics of the specimen in the LMFT is shown in **Figure 13**.

Setting of the model is:

(I)   Specimen is in the free space (vacuum).

(II)   Specimen thickness $d \gg \lambda$. This means that negative surface tension of S/V (V stands for vacuum) interfaces due to nonzero $H_\parallel$ is neglected.

(III)   Longitudinal sizes of the specimen (along x and y axes) are much greater than thickness d, i.e., the slab is considered infinite. This means that flux of the perpendicular component of the applied field $H_\perp$ is conserved, and therefore $H_\perp = \overline{B}_\perp = B_\perp \rho_n$, where $\overline{B}_\perp$ is average perpendicular component of the induction over the specimen, $B_\perp$ is perpendicular component of the induction in N domains (considered uniform), and ρ_n is volume fraction of the N phase: $\rho_n = D_n/D = V_n/V$ with D_n and V_n designating the width of the N laminae and a total volume of the N phase, respectively.

(IV) $B_\parallel = (H_i)_\parallel = H_\parallel$ due to the absence of the demagnetizing field along y-axis or along the parallel component of the applied field $H_\parallel$.

(V)   Tinkham's version of the FDDS (see **Figure 5C**) is adopted due to its simplicity and consistency with the experimental images.

We start from construction of a thermodynamic potential $\tilde{F}(T, V, H_i)$, which is the Legendre transform of the Helmholtz free energy $F(T, V, B)$ to the variables (T, V, H_i). It is often referred to as the Gibbs free energy[4]:

$$\tilde{F} = F - \frac{\mathbf{B} \cdot \mathbf{H}_i}{4\pi} V = F - \frac{B_\parallel H_{i\parallel}}{4\pi} V - \frac{B_\perp H_{i\perp}}{4\pi} V = F - \frac{B_\parallel H_{i\parallel}}{4\pi} V = F - \frac{H_\parallel^2}{4\pi} V, \qquad (13)$$

where $F(T, V, B)$ is Helmoltz free energy. The term $(\mathbf{B} \cdot \mathbf{H}_i/4\pi)V$ reflects work done by the magnet power supply to keep the set field H when the flux in the system changes [2]. In our case the flux of the perpendicular component is fixed, and therefore the term $(B_\perp H_{i\perp}/4\pi)V$

---

[4]It should be remembered that canonical Gibbs free energy is function of pressure, but not volume, as in this case.
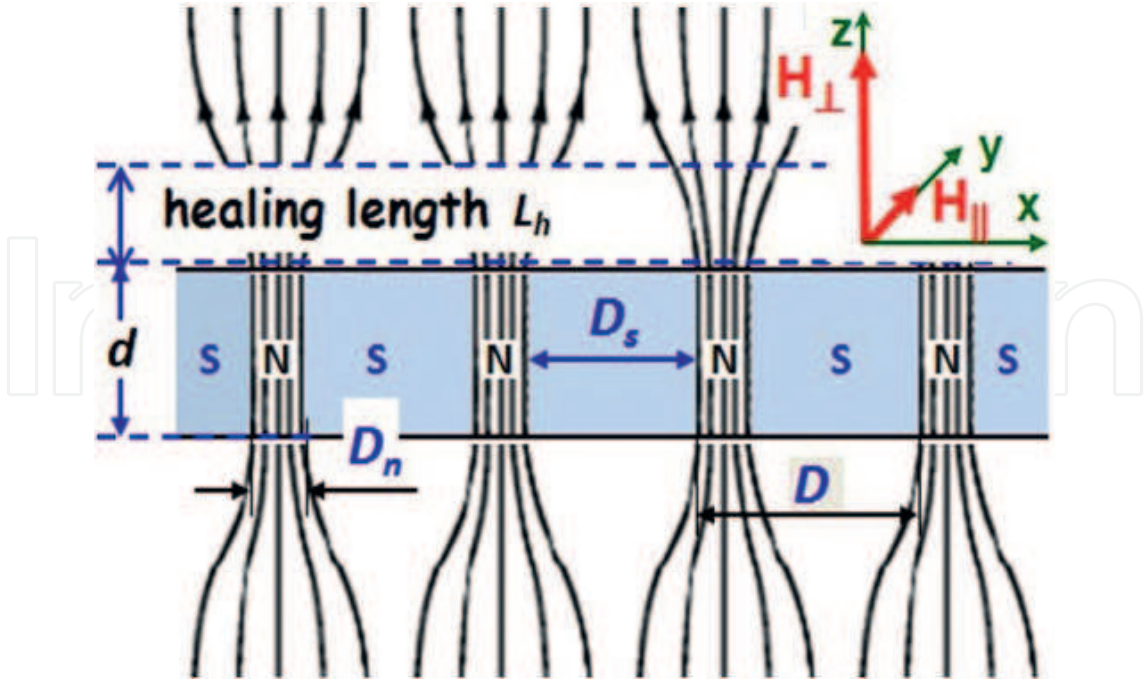
Figure 13. Cross-sectional view of the specimen/field configuration in the laminar model for tilted field. $H_\parallel$ and $H_\perp$ are parallel and perpendicular components of the applied field, respectively. Domains are rectangular parallelepipeds extended along $H_\parallel$ (y-axis). The healing length L_h is the characteristic distance over which the disturbed field relaxes to the uniformly distributed state. In N domains the parallel component of the induction $B_\parallel = H_\parallel$, while the perpendicular component $B_\perp = H_\perp/\rho_n$, where $\rho_n = D_n/D = V_n/V$ is volume fraction of the N phase and V_n is the total volume of the N phase. After Kozhevnikov et al. [26].

drops out. On that reason in pure perpendicular field, $\tilde{F} = F$ [2, 3, 8]. On the other hand, $H_{i\parallel} = H_\parallel$, due to the specimen geometry (see setting (iv) above).

To transform $\tilde{F}(T, V, H_i)$ to the total free energy $\tilde{F}(T, V, H)_M$, we need to add terms associated with energy of interaction of the applied field H with the specimen. In pure parallel case, this term is $+(H^2/8\pi)V$ [2]. In pure perpendicular case, it is $-(H^2/8\pi)V$ (see appendix in [26] and/or [2]). Therefore in our case the total free energy of the specimen is

$$\tilde{F}_M = \tilde{F} + \left[\frac{H_\parallel^2}{8\pi} - \frac{H_\perp^2}{8\pi} \right] V. \tag{14}$$

Now, summing:

a.   Free energy at zero field $V[f_{n0} - H_c^2(1 - \rho_n)/8\pi)]$, where $f_{n0} = F_{n0}/V$ is free energy density of the N state in zero field.

b.   Energy of the field B in the N domains $V\rho_n \left(B_\perp^2 + B_\parallel^2 \right)/8\pi$.

c.   Energy of the S/N interfaces $2VH_c^2\delta/8\pi D$.

d.   Excess energy of the field over the healing length $2VL_h \left(\rho_n B_\perp^2 - H_\perp^2 \right)/8\pi d$, and plugging all in Eq. (14), one obtains for $\tilde{f}_M = \tilde{F}_M/V$:

$$\tilde{f}_M = f_{n0} - (1 - \rho_n)\frac{H_c^2}{8\pi} + \frac{H_\perp^2}{8\pi\rho_n} - \rho_n\frac{H_\parallel^2}{8\pi} + 2\frac{H_c^2}{8\pi}\frac{\delta}{D} + 2\frac{H_\perp^2}{8\pi}\frac{D}{d}(1 - \rho_n)^2 + \frac{H_\parallel^2}{8\pi} - \frac{H_\perp^2}{8\pi}. \tag{15}$$

Then, minimizing $\tilde{f}_M$ with respect to D, one finds equilibrium period of the structure

$$D^2 = \frac{d\delta}{\rho_n^2(1 - \rho_n)^2}\frac{H_c^2}{B_\perp^2} = \frac{d\delta}{(1 - \rho_n)^2}\frac{H_c^2}{H_\perp^2}. \tag{16}$$

After plugging this optimal D into Eq. (15), the latter takes form:

$$\tilde{f}_M = f_{n0} - \frac{H_c^2}{8\pi}(1 - \rho_n)\left[1 - h_\parallel^2 - \frac{h_\perp^2}{\rho_n} - 4h_\perp\sqrt{\frac{\delta}{d}}\right], \tag{17}$$

where $h_\perp$ and $h_\parallel$ are reduced components of the applied field $H_\perp/H_c$ and $H_\parallel/H_c$, respectively. Important to note that with the optimal D the terms related to the S/N interfaces and to the field inhomogeneity near the surface are equal. This means that "responsibility" for deviation of the properties of real specimens from those in the PL model is equally shared between these two contributions in the specimen free energy.

Minimizing $\tilde{f}_M$ with respect to ρ_n, one finds equilibrium volume fraction of the N component:

$$\rho_n^2 = h_\perp^2 / \left(1 - 4h_\perp\sqrt{\delta/d} - h_\parallel^2\right). \tag{18}$$

At the IS/N transition ρ_n=1, hence

$$h_{cr\perp} = \sqrt{4(\delta/d) + 1 - h_\parallel^2} - 2\sqrt{\delta/d}. \tag{19}$$

And magnitude of the reduced induction $b = B/H_c$ in the N domains is

$$b^2 = b_\perp^2 + b_\parallel^2 = h_\perp^2/\rho_n^2 + h_\parallel^2 = 1 - 4h_\perp\sqrt{\delta/d}. \tag{20}$$

Before calculating the magnetic moment, we transform Eq. (17) substituting ρ_n from Eq. (18) and using $b_\perp$ from Eq. (20): $b_\perp^2 = 1 - 4h_\perp\sqrt{\delta/d} - h_\parallel^2$. Then Eq. (17) becomes very compact:

$$\tilde{f}_M = f_{n0} - \frac{H_c^2}{8\pi}(b_\perp - h_\perp)^2 = f_{n0} - \frac{B_\perp^2}{8\pi}(1 - \rho_n)^2. \tag{21}$$

Now one can calculate the specimen magnetic moment from the definitive relationship Eq. (3):

$$\mathbf{M} \equiv -\nabla_H(\tilde{F}_M) = -\left(\frac{\partial\tilde{F}_M}{\partial H_\parallel}y + \frac{\partial\tilde{F}_M}{\partial H_\perp}z\right), \tag{22}$$

where y and z are unit vectors along the y and z axes, respectively.

The first term in Eq. (22) is

$$\frac{\partial \tilde{F}_M}{\partial H_\parallel} = \frac{V}{H_c} \cdot \frac{\partial \tilde{f}_M}{\partial h_\parallel} = \frac{V}{H_c} \cdot \frac{H_c^2}{8\pi} \, 2\,(b_\perp - h_\perp) \frac{\partial b_\perp}{\partial h_\parallel}. \tag{23}$$

Since $\partial b_\perp / \partial h_\parallel = h_\parallel / b_\perp$ (see Eq. (20)), the final form of the parallel component of the specimen magnetic moment is

$$-M_\parallel = \frac{\partial \tilde{F}_M}{\partial H_\parallel} = \frac{V}{H_c}\frac{H_c^2}{8\pi}\, 2\,(b_\perp - h_\perp)\frac{h_\parallel}{b_\perp} = \frac{V H_c}{4\pi}\left(1 - \frac{h_\perp}{b_\perp}\right)h_\parallel = \frac{V}{4\pi}\,(1 - \rho_n)H_\parallel. \tag{24}$$

And the perpendicular component of the moment is

$$-M_\perp = \frac{\partial \tilde{F}_M}{\partial H_\perp} = \frac{V}{H_c}\frac{\partial \tilde{f}_M}{\partial h_\perp} = -\frac{V}{H_c}\frac{2H_c^2}{8\pi}\,(b_\perp - h_\perp)\left(\frac{\partial b_\perp}{\partial h_\perp} - 1\right) = \frac{V}{4\pi}\,(1 - \rho_n)\left(1 - \frac{\partial B_\perp}{\partial H_\perp}\right)B_\perp. \tag{25}$$

All obtained formulas are analyzed in detail in [25, 26], where it is shown that the model correctly describes experimental data. In particular, the coherence length calculated from measured D using Eq. (16) agrees well with that obtained from the magnetic field profile measured in [36]. Here we confine our discussion by limiting cases.

In *parallel field* ($H_\perp = 0$) the model (Eq. (18)) yields $\rho_n = 0$, meaning that the specimen is in the Meissner state where the N phase is absent. Then $\tilde{f}_M$ (Eq. (17)) converts to Eq. (5):

$$\tilde{f}_M = f_n - \frac{H_c^2}{8\pi}\,(1 - h^2) = f_n - \frac{H_c^2}{8\pi} + \frac{H^2}{8\pi}, \tag{26}$$

and $M = M_\parallel$ (Eq. (24)) converts to Eq. (1):

$$M_\parallel = M = -\frac{V}{4\pi}H. \tag{27}$$

In *perpendicular field* ($H_\parallel = 0$) one can see that $h_{cr}(= h_{cr\perp})$ decreases with decreasing thickness d (Eq. (19)) in accord with the experimental data [25, 26, 33], and the induction $B(= b \cdot H_c)$ in N domains equals to H_c at $H = H_I = 0$ and decreases with increasing H (Eq. (20)), as it was found experimentally in [34]. For magnetization $4\pi M/V$ at $H \to 0$, when $\rho_n = 0$, the model (Eq. (25)) yields

$$\frac{4\pi M(0)}{V} = \frac{V}{4\pi}\left(1 - \frac{\partial B_\perp}{\partial H_\perp}\right)H_c. \tag{28}$$

Since B decreases with increasing H, $(\partial B_\perp / \partial H_\perp) < 0$, and therefore the expression in parentheses is greater than unity. This makes $4\pi M(0)/V$ greater than H_c, thus explaining appearance of the excess magnetization at H_I as it is seen, e.g., in **Figures 9** and **12**.

The infinite slab in perpendicular field represents ellipsoid with $\eta = 1$. If the slab is thick (i.e., $d \gg \delta$), the LMTF model converts to the PL model for specimens with unity demagnetization.

Specifically, in the thick slabs $\rho_n = H/H_c$ (Eq. (18)), and therefore (a) $B = (h/\rho_n)H_c = H_c$ and $H_i = B/\mu = H_c$, and (b) $4\pi M/V = -H_c + H$, meaning that $4\pi M(0)/V = -H_c$ and $H_{cr} = H_c$, exactly as it takes place in the PL model (**Figure 4b**). The third condition of Eq. (11) $\overline{B} = H$ follows from the law of the flux conservation always valid for infinite slabs. Thus the LMTF model explains why the PL model works the best for thick specimens: because in such case combined contributions due to near-surface field inhomogeneity and due to the S/N interfaces (both are characterized by the ratio δ/d) are negligible compared to the bulk terms in Eqs. (15) and (17).

Now, when we are convinced in correctness of the formulas for magnetization (see more in [25, 26]), we can rewrite Eq. (17) in its canonical form coinciding with the mandatory form for the total free energy Eq. (4):

$$\tilde{F}_M = \tilde{F}_M(H = 0) - \int_0^H \mathbf{M} \cdot d\mathbf{H} = F_{s0} - \int_0^H \mathbf{M} \cdot d\mathbf{H} = F_{n0} - \frac{H_c^2}{8\pi}V - \int_0^H \mathbf{M} \cdot d\mathbf{H} \qquad (29)$$

where the components of $\mathbf{M}$ are given by Eqs. (24 and 25).

7. Concluding remarks

More than three decades starting from the 1930s, the problem of the IS was in the main focus of experimental and theoretical researches on superconductivity. This resulted in significant progress reached in understanding properties of the IS as well as properties of superconducting state as a whole. Excellent reviews of these researches are available in [1, 12]. However some puzzles in the IS properties remained open until their possible explanations emerged in studies of recent years. In this chapter we mostly focused at results of these studies.

In particular, we discussed a recently developed phenomenological model of the IS composed for infinite slabs in arbitrary tilted magnetic field. Naturally, this model is not and cannot be free of disadvantages. One of them can be associated with the use of an oversimplified Tinkham approximation for the field distribution and domain shape near the surface through which the flux enters and leaves the specimen. We believe that modern experimental capabilities associated, e.g., with muon spectroscopy and noninvasive scanning magnetic microscopy, can help to resolve this important and very interesting issue, which we discussed in the Section IV. The new model discussed in Section VI is restricted by the slab-like specimens. Its extension to all ellipsoidal shapes covered in the model of Peierls and London is another possible avenue of research on the IS.

Finally, it is important to remind that the IS is one of two inhomogeneous superconducting states. The second state is the mixed state in type-II superconductors, taking place in vast majority of superconducting materials, including those used in practical applications. Therefore understanding of properties of the IS can help to understand properties of the mixed state. As an example, the field distribution and shape of the normal domains (vortices in type-II materials) near the specimen surface should be similar in both these inhomogeneous states.

Author details

Vladimir Kozhevnikov

Address all correspondence to: vladimir@itf.fys.kuleuven.be

Tulsa Community College, Tulsa, Oklahoma, USA

References

[1] Shoenberg D. Superconductivity. 2nd. ed. Cambridge: Cambridge University Press; 1952

[2] Landau LD, Lifshitz EM, Pitaevskii LP. Electrodynamics of Continuous Media. 2nd ed. Amsterdam: Elsevier; 1984

[3] Tinkham M. Introduction to Superconductivity. Mineola: Dover Publication; 1996

[4] Maxwell JC. A Treatise on Electricity and Magnetism. 2nd ed. Vol. II. Oxford: Clarendon Press; 1881

[5] Jackson JD. Classical Electrodynamics. 3d ed. Hoboken NJ: JohnWiley and Sons; 1999

[6] Purcell EM. Electricity and Magnetism. Boston MA: McGraw-Hill; 1985

[7] Abrikosov AA. Fundamentals of the Theory of Metals. Amsterdam: Elsevier Science Pub. Co.; 1988

[8] De Gennes PG. Superconductivity of Metals and Alloys. Boulder, CO: Westview; 1966

[9] Tamm IE. Fundamentals of the Theory of Electricity. Moscow: Mir; 1979

[10] Gorter CJ, Casimir H. Physica. 1934;**1**:306

[11] Peierls R. Proceedings of the Royal Society of London. Series A. 1936;**155**:613

[12] Livingston JD, DeSorbo W. In: Parks RD, editor. Superconductivity II. N.Y.: Marcel Dekker; 1969. p. 1235

[13] Huebener RP. Magnetic Flux Structures in Superconductors. 2nd ed. N.Y.3: Springler-Verlag; 2010

[14] Brandt EH, Das MP. Journal of Superconductivity and Novel Magnetism. 2001;**24**:57

[15] Clem JR, Prozorov R, Wijngaarden RJ. Physical Review B. 2013;**88**:104504

[16] London F. Physica. 1936;**3**:450

[17] Kozhevnikov V, Valente-Feliciano A-M, Curran PJ, Richter G, Volodin A, Suter A, Bending S J, Van Haesendonck C. Journal of Superconductivity and Novel Magnetism. 2018. https://doi.org/10.1007/s10948-018-4622-y

[18] Landau LD. ZhETF. 1937;**7**:371

[19] Landau LD. ZhETF. 1943;**13**:377

[20] Marchenko VI. ZhETF. 1976;**71**:2194

[21] Lifshitz EM, Sharvin YV. Doklady Akademii Nauk SSSR. 1951;**79**:783

[22] Fortini A, Paumier E. Physical Review B. 1972;**5**:1850

[23] Landau LD. Nature. 1938;**141**:688

[24] Meshkovsky AG, Shalnikov AI. ZhETF. 1947;**17**:851

[25] Kozhevnikov V, Wijngaarden RJ, de Wit J, Van Haesendonck C. Physical Review B. 2014;**89**(R):100503

[26] Kozhevnikov V, Van Haesendonck C. Physical Review B. 2014;**90**:104519

[27] Neidermayer C, Forgan EM, Gluckler H, Hofer A, Morenzoni E, Pleines M, Prokscha T, Riseman TM, Brike M, Jackson TJ, Litterst J, Long MW, Luetkens H, Schatz A, Schatz G. Physical Review Letters. 1999;**83**:3932

[28] Andrew ER. Proceedings of the Royal Society of London A. 1948;**194**:80

[29] de HaasWJ, Voogd J. Communications from the Laboratory of Physics of the University of Leiden, 1931:214d

[30] de HaasWJ, Voogd J, Jonker JM. Physica.1934;**1**:281

[31] Faber IT. Proceedings of the Royal Society of London. Series A. 1958;**248**:460

[32] Sharvin YV. ZhETF. 1957;**33**:1341

[33] Sharvin YV. ZhETF. 1960;**38**:298

[34] Desirant M, Shoenberg D. Proceedings of the Royal Society of London A. 1948;**194**:63

[35] Egorov VS, Solt G, Baines C, Herlach D, Zimmermann U. Physical Review B. 2001;**64**:024524

[36] Kozhevnikov V, Valente-Feliciano A-M, Curran PJ, Suter A, Liu AH, Richter G, Morenzoni E, Bending SJ, Van Haesendonck C. Physical Review B. 2017;**95**:174509

[37] Kozhevnikov V, Suter A, Fritzsche H, Gladilin V, Volodin A, Moorkens T, Trekels M, Cuppens J, Wojek BM, Prokscha T, Morenzoni E, Nieuwenhuys GJ, Van Bael MJ, Temst K, Van Haesendonck C, Indekeu JO. Physical Review B. 2013;**87**:104508